$3s2p$ inelastic x-ray scattering of CaF_2

F. M. F. de Groot
Solid State Physics, University of Groningen, Nijenborgh 4, 9747 AG Groningen, The Netherlands
(Received 17 August 1995; revised manuscript received 14 November 1995)

In this paper the $3s2p$ inelastic x-ray scattering (IXS) cross sections of CaF_2 are analyzed using a ligand-field multiplet approach. All dipole matrix elements necessary for the IXS cross section are calculated and it is shown that interference effects are not negligible. The important possibility to map out a specific character of the $2p^5 3d^1$ intermediate states is explained. The experimental results of Rubensson *et al.* are reproduced with the ligand field multiplet model and the Kramers-Heisenberg equation of inelastic x-ray scattering. The values found for the ligand-field splitting (-0.91 eV) and the $3s3d$ exchange splitting (1.2 eV) differ from the results fitted to experiment.

I. INTRODUCTION

In the last five years a wealth of experimental data has been gathered on core spectroscopies of CaF_2. With the improvement of the resolution of soft x-ray monochromators at synchrotron radiation sources,[1] sharp-structured x-ray absorption spectra were obtained. In fact the structures obtained [with a Lorentzian broadening of only 80 meV in case of the lowest energy peaks of CaF_2 (Ref. 2)] are in many cases sharper than the tabulated core hole lifetime broadenings.[3] CaF_2 has been a much studied system for at least two reasons: (1) it can be considered as a prototype system in many theoretical approaches and serves to test the theoretical predictions and also to develop the theoretical models into the new field of high-resolution spectra; (2) the interfaces of CaF_2 with Si and GaAs are important for applications in the semiconductor industry and also the study of these interfaces reached new openings in the understanding of interfaces in general, partly due to the possibility to prepare high-quality interfaces.[4] In the present paper for all property (1) is important, that is the electronic structure of CaF_2 is simple to explain: CaF_2 is rather ionic and has a large band gap of approximately 12 eV. The valence band is formed by the fluorine $2p$ band and the first empty ''band'' contain the $3d$ states. This is not to say that the valence band is 100% pure F $2p$ and in fact there is some admixture of Ca $3d$, $4s$, and $4p$ character, as quantified by band structure calculations.[5,6] However, an important aspect that is implied is that the valence band consists of six electron states and there is a large gap to the ten hole states originating from the $3d$ band and further hole states due to the other empty bands.

The valence band has been studied with photoemission and with $3p$ resonant photoemission ($3p$ RPES). Its width, at half maximum height, is approximately 3.3 eV and the maximum dispersion of the peak position is only 2.3 eV.[4] In this same paper the first ''high-resolution'' $2p$ x-ray absorption spectra were published, with an initial analysis in which the seven peaks observed were described qualitatively (and as turned out later, not completely correct) to a combination of multiplet effects and interface effects. The quantitative interpretation of the $2p$ x-ray absorption spectrum revealed that there are indeed seven transitions possible, but two are too close to be separated so six peaks are observable.[2] A study of Himpsel and co-workers showed that the seventh observable peak is related to an intrinsic surface effect due to the relatively shallow probing depth of electron-yield detection.[7] The seven possible final states relate to the seven multiplet states of the $2p^5 3d^1$ final state. As has been described in detail[2] this $2p^5 3d^1$ state is subject to large multiplet effects caused by the strong $2p3d$ Coulomb and exchange interactions. The multiplet effects dominate the other energy effects due to the ligand field and the $2p$ spin-orbit coupling. The $3d$ spin-orbit is weak (8 meV) and its inclusion does not modify the picture presented. For a detailed analysis of the symmetry effects the readers is referred to Refs. 2 and 8.

Only recently has the $2p$ excitation been used to resonantly enhance photoemission processes.[9] $2p$ RPES has been used to study the valence band,[10–15] but also shallow core excitations like $3s$ and $3p$ have been studied at the $2p$ resonance.[15–18] The $2p$ hole state gives also rise to resonances in Auger channels like $2p3p3p$ resonant Auger electron spectroscopy (RAES).[16,19] The mechanism for both RPES and RAES is identical and both occur due to two-electron Auger matrix elements. Their only difference is that the photoemission final states can be reached directly by dipole transitions from the ground state. The possible RAES final states are $\underline{3s}\,\underline{3s}$, $\underline{3s}\,\underline{3p}$, and $\underline{3p}\,\underline{3p}$ two-hole states, all with the presence of the excited $3d$ electron. The RPES final states are the one-hole states $\underline{3s}$ and $\underline{3p}$. In case of CaF_2 the $3d$ band is empty and $3d$ RPES does not occur. With respect to the interpretation of $2p$ RPES experiments there is a debate regarding the question if there ''exists'' any resonance.[12] In the one interpretation there is, in contrast to $3p$ RPES, no resonance effect and one observes a mere addition of the photoemission channel and the indirect ''Auger'' channel.[12] This viewpoint might seem somewhat strange if one realizes that one is considering in the RPES process a situation in which the initial and final states are identical and in which two paths exist between them. It might be possible that these effects are too small to be observed, as apparently they are in some cases. What one is effectively discussing are two mechanisms for the decay of a ''$2p$ core hole,'' or better the $2p3d$ exciton. There are many decay routes of a $2p3d$ exciton, i.e., the various radiative and nonradiative decay channels. For the problem as sketched above it is important to

divide these channels into two classes. One class fills the $2p$ hole and the other class modifies the state but leaves a $2p$ hole present. To this second category belong the so-called Coster-Kronig Auger channels that describe the decay of a $2p_{1/2}$ hole into a $2p_{3/2}$ hole. As has been argued in Ref. 19 such decay channels can in principle occur also within the $2p_{3/2}$ (L_3) edge. The $2p \rightarrow 2p'$ Auger decay channels, which might be indicated with terms like ''dephasing'' or ''relaxation,'' leave the system in an ionized state. If such channels dominate the intermediate state changes its nature (i.e., its number of electrons) with the consequence that the final state reached is not identical to the one reached directly by photoemission, thereby removing the interference effects. Thus the debate might be rendered a debate as to whether ''dephasing'' or ''core hole decay'' dominates. In fact for several systems this question can be partly answered from an analysis of, for example, their $2p3p3p$ RAES spectral shapes. As shown in the data of Elango and co-workers,[16] in case of the $2p3p3p$ RAES of CaF_2 ''core-hole decay'' dominates, but for the $2p_{1/2}$ states the effects of dephasing, followed by normal Auger, are clearly visible. The debate started with the interpretation of metallic systems such as Ni, which are much more ''covalent'' and for which indeed the dephasing will be more important and likely to be dominant.[12] However, the effects of resonant core-hole decay have been shown to exist too.[13] The dynamics of nonradiative decay is also important for the interpretation of the inelastic x-ray scattering cross sections (see Sec. III).

Many different names are used to denote the process in which one comes in with a photon of energy ω, detecting a photon with energy ω'. Names used include core-core inelastic x-ray scattering (core-core) resonant Raman scattering, resonant x-ray emission,[20] and threshold-excited soft x-ray fluorescence.[21] The process obviously is an inelastic scattering process, but to distinguish the present process from other inelastic x-ray scattering (IXS) processes one can add the label ''core-core'' (or specifically $3s2p$), or alternatively use the label ''Raman,'' which denotes a resonant process via a localized electronic state. The equivalent terms resonant x-ray emission and threshold-excited soft x-ray fluorescence denote the close relation to resonant photoemission. They are derived from the experimental situation for which the x-ray emission (fluorescence) cross section is measured at a series of excitation energies close to an x-ray absorption edge.

The study of core-core inelastic x-ray scattering experiments is a rather new field. Due to the low cross sections a large number of photons is necessary to obtain sufficiently accurate experimental data. Hämäläinen *et al.* measured the $3p1s$ inelastic x-ray scattering cross sections of manganese systems[22] and the $4d2p$ IXS spectra for dysprosium.[23] For the $3p1s$ IXS spectra it has been determined that (1) the $1s$ lifetime broadening disappears and (2) one can use two different decay channels and separate spin up and spin down in a so-called ''local-spin-selective'' x-ray absorption experiment. The use of a $1s$ core state for the resonance has some important consequences such as the absence of interference effects, essentially because there is only one core state (per spin) that resonates.[24] This is not the case for the $4d2p$ IXS spectra of rare earths as discussed by Carra, Fabrizio, and Thole.[25] Also in the present case of $3s2p$ IXS interference effects will be important.

The $3s2p$ IXS spectra of CaF_2 have been measured recently by Rubensson *et al.*[21] Their findings will be discussed in Sec. III, where a comparison will be made of the theoretical results with these experiments. In Sec. II the theoretical procedure is outlined.

II. THEORY

The $3s2p$ inelastic x-ray scattering cross section is dominated by resonant scattering via the $2p^5 3d^1$ intermediate states. This reduces the calculation to the transitions of $3d^0$, via $2p^5 3d^1$, to $3s^1 3d^1$ states. The effects of charge transfer are small and will be neglected. They are discussed in Sec. III. Both the x-ray absorption and x-ray emission steps conserve the local charge and it has been shown that in those experimental conditions ionic systems like CaF_2 can be described in close detail by the ligand field approximation.[2,8]

Inelastic scattering from localized core states can be described with the so-called generalized Kramers-Heisenberg formula:[26,27]

$$I(\omega,\omega') = \sum_f \left| \sum_x \frac{\langle f|r_q|x\rangle\langle x|r_q|i_0\rangle}{E_{i_0}+\omega-E_x-i\Gamma_x} \right|^2 L_f(\omega-\omega') G_E , \tag{1}$$

with ω and ω' as, respectively, the incoming and outgoing x-ray energies. i_0 represents the $3d^0$ ground state, x the $2p^5 3d^1$ intermediate states, and f the $3s^1 3d^1$ final states. All angular (polarization) degrees of freedom have been taken from Eq. (1).[27] L_f indicates a Lorentzian broadening of the $3s^1 3d^5$ final states and G_E the experimental broadening, which is approximated with a Gaussian. For the present case of $3s2p$ inelastic x-ray scattering it is important to calculate the dipole matrix elements $\langle 3s^1 3d^1[\Gamma']|r_q|2p^5 3d^1[\Gamma]\rangle$ and $\langle 2p^5 3d^1[\Gamma]|r_q|3d^0\rangle$. The denominator indicates that a resonance occurs if the incoming x-ray energy (ω) equals the energy difference between the intermediate state (E_x) and the ground state (E_{i_0}). Interference effects are important because the energy separation between the intermediate states is of the same order of magnitude as their lifetime broadening (Γ_x).

First the symmetries of the states and their respective energies are discussed, followed by a section on the actual calculation of the necessary matrix elements and with Eq. (1) of the resulting IXS cross sections.

A. Symmetries

Starting from a situation with all bands completely full or empty has the advantage of strong restrictions on the possible symmetry states. Important ingredients for the possible symmetries are the dipole selection rule, the projection rules for different symmetry groups, and the multiplication rules used to combine symmetries of two electrons or used to combine the L and S symmetry states with spin-orbit coupling. For readers not familiar with group theory these rules are briefly introduced in the Appendix.[28]

Ligand field multiplet calculations have been performed for the $3d^0$ initial state, the $2p^5 3d^1$ intermediate states, and

TABLE I. The respective symmetries of the configurations involved for the ground state, intermediate states, and final states. All states in boldface can be actually reached from the $[A_1]$ ground state symmetry, via, respectively, one and two dipolar transitions.

Configuration	Atomic symmetries	Cubic symmetries (LS)	Cubic symmetries [J]
$3d^0$	^1S	$^1(A_1)$	$[A_1]$
$\downarrow$			$[A_1]\otimes[T_1]=[T_1]$
$2p^5 3d^1$	$^2P\otimes{}^2D$	$^{1,3}(T_1T_2T_1T_2EA_2)$	$[\mathbf{T_1}],[T_2],[\mathbf{T_1}],[T_2],[E],[A_2]$ $[\mathbf{T_1}T_2EA_1],[\mathbf{T_1}T_2EA_2],[\mathbf{T_1}T_2EA_1]$ $[\mathbf{T_1}T_2EA_2],[\mathbf{T_1}T_2],[T_2]$
$\downarrow$			$[T_1]\otimes[T_1]=[A_1ET_1T_2]$
$3s^1 3d^1$	$^2S\otimes{}^2D$	$^{1,3}(ET_2)$	$[\mathbf{E}],[\mathbf{T_2}],[\mathbf{T_1T_2}],[\mathbf{T_1T_2E}A_2]$

the $3s^1 3d^1$ final states in cubic symmetry. The respective symmetries of the configurations in atomic and cubic symmetries are given in Table I. The cubic symmetries are given with their LS-like term symbols ^{2S+1}L, where L is given with the Schönfliess notation of its irreducible representation. To specify completely the symmetry states it is necessary to project also the S quantum numbers to cubic symmetry and to couple the spin and orbit representations to J-like total symmetry representations. All total symmetry representations are given with square brackets.

The $3d^0$ initial state consists of only one state with $L=S=J=0$ giving a cubic symmetry of $^1A_1[A_1]$. The $2p^5 3d^1$ intermediate states have the atomic symmetries given by the multiplication of ^2P times ^2D, yielding singlet and triplet states of P, D, and F. The change from atomic (SO_3) to cubic (O_h) symmetry projects P to T_1 and splits D into E and T_2. (cf. Appendix). Multiplying the representations of both electrons yields the singlet and triplet states of, respectively, T_1, T_2, T_1, T_2, E, and A_2 symmetry. This gives a total number of 25 different total symmetry states. It can be checked (from the Appendix) that these are respectively, 2 states of $[A_1]$ symmetry, 3 $[A_2]$ states, 5 $[E]$ states, 7 $[T_1]$ states and 8 $[T_2]$ states. All these 25 states are possible within the $2p^5 3d^1$ state in cubic symmetry, but they cannot all be reached from the ground state. Which symmetries do have a finite transition strength depends on the dipole selection rules. As the ground state has symmetry $[A_1]$ the only possible states reachable with a dipole transition must have $[T_1]$ symmetry and only 7 of the 25 states acquire intensity. They are indicated with boldface in Table I. The $3s^1 3d^1$ final states are found by multiplying ^2S with ^2D. Within cubic symmetry these states are projected to 8 states as given in Table I. From these 8 states only the $[A_2]$-symmetry states *cannot* be reached by the dipole selection rule from the $[T_1]$ symmetry intermediate states.

B. Energies

The respective energies of the different symmetry states have been calculated using a Hartree-Fock-based program. The initial state consists of a single symmetry and its energy is set to zero. The relative energies of the $3s^1 3d^5$ final states are determined by the $3s3d$ exchange integral, the ligand field splitting, and the $3d$ spin-orbit coupling. The $3s3d$ exchange integral splits the states into triplets and singlets and the ligand field splits the states of T_2 and E symmetry. Both the $3s3d$ exchange splitting and the ligand field splitting are of the order of 1 eV and they give rise to 4 states, given in LS symmetry by, respectively, ^3E, $^3T_2$, ^1E, and $^1T_2$. The spin-orbit coupling of the $3d$ electron (ζ_d) is very small for divalent calcium, only 8 meV. For atomic symmetries the ^3D state is split into $^3D_3$, $^3D_2$, and $^3D_1$ separated by, respectively, $\frac{3}{2}\zeta_d$ and ζ_d. Due to the ligand field the $3d$ spin-orbit coupling is partly quenched, from a $J=2$ state to an effective $J=1$ state. The $3d$ spin-orbit coupling splits the $^3T_2$ state into, respectively, $[T_1]$, $[E]$, $[T_2]$, and $[A_2]$ total symmetry states. The energy differences between $[T_1]+[E]$ and $[T_2]$ equals the $3d$ spin-orbit coupling, while the energy difference between $[T_2]$ and $[A_2]$ is equal to $\frac{1}{2}\zeta_d$. These energy separations occur for all cases where the ligand field strength is considerably larger than the $3d$ spin-orbit coupling. The ^3E state is split into $[T_1]$ and $[T_2]$ but their energies are equal.

The situation for the $2p^5 3d^1$ intermediate states is similar and the states are split by the ligand field, $2p3d$ exchange, and the small $3d$ spin-orbit coupling. An important difference, however, is that the $2p3d$ exchange integral is large and takes a more complex form. This has been described in detail in the analysis of the $2p$ x-ray absorption spectral shape.[2] For a $2p3d$ interaction the ''exchange'' integral is written with three Slater integrals F^2, G^1, and G^3 which are of the order of 10 eV. They cause the occurrence of small ''prepeaks'' and a complete reordering of the intensities of the various peaks.

C. Matrix elements and IXS cross sections

The calculations have been performed with the COWAN (Ref. 29) and BUTLER (Ref. 30) computer codes, describing,

TABLE II. Parameters used in the ligand field multiplet calculation. The ligand field value has been optimized to the $2p$ x-ray absorption spectral shape. All Slater integrals have been reduced to 80% of their HF value. The actual $3s3d$ exchange splitting is equal to $\frac{2}{5}G^1$.

Parameter	Origin
$2p^5 3d^1$	Intermediate states:
$\zeta_p = 2.4$ eV	HF calculation
$\zeta_d = 11$ meV	HF calculation
$F^2 = 3.03$ eV	HF calculation
$G^1 = 2.01$ eV	HF calculation
$G^3 = 1.14$ eV	HF calculation
$10Dq = -0.91$ eV	Set to experiment
$3s^1 3d^1$	Final states:
$\zeta_d = 8$ meV	HF calculation
$G^1 = 3.00$ eV	HF calculation
	Splitting of 1.2 eV
$10Dq = -0.91$ eV	Splitting of 0.91 eV

respectively, the atomic multiplets and their projection to cubic symmetry.[8] The COWAN program calculates the average energies of the $3d^0$, $2p^5 3d^1$ and $3s^1 3d^1$ configurations. The absolute energies resulting from the Hartree-Fock-(HF-)based program are off by some eV. To make a close comparison to the experiments in the remainder of this paper the absolute energies of the configurations have been set to experiment. That is the energy position of the highest-energy peak in the $2p$ x-ray absorption spectrum has been set to 352.3 eV and the energy position of the highest-energy peak in the $3s2p$ IXS spectrum has been set to 48.64 eV.[21] The parameters used in the ligand field multiplet model are given in Table II. They are exactly the same as in Ref.2, where it has been shown that they reproduce the $2p$ x-ray absorption spectrum of CaF_2 in great detail.

In order to determine all possible matrices the seven transitions $3d^0 \rightarrow 2p^5 3d^1[\Gamma]$ must be calculated for the excitation. The decay step is described with a 7×7 matrix for all transitions $2p^5 3d^1[\Gamma] \rightarrow 3s^1 3d^1[\Gamma']$. Table III gives all energy-positions of the intermediate and final states and all matrix elements. The first column gives the $2p^5 3d^1$ energies and the second column the ''x-ray absorption'' matrix element. The other columns contain the decay matrix elements between the seven intermediate states and the seven final states, which are indicated at the top. The matrix elements do have a positive or negative sign, important for the interference effects. The overall intensity of each of the seven excitation states integrated over the decay channels is equal and also the intensities to each of the seven final states integrated over the intermediate states is equal. This comes about as the overall intensity originates from the $3s \rightarrow 2p$ transition. The details of the $2p3d$ and $3s3d$ couplings give the spectral shapes but do not alter the overall intensity. Table III contains the information necessary to determine the inelastic x-ray cross sections. Additional parameters needed are the $2p$ lifetime broadening (Γ_{2p}), the $3s$ lifetime broadening (Γ_{3s}), and for the simulation of experiments also the spread of the incoming and outgoing x-ray energies, both assumed to be Gaussians.

An approximate picture to describe the IXS cross sections is to assume that they are given as the $2p$ x-ray absorption cross section multiplied for each intermediate state by the various $3s2p$ x-ray emission cross sections. This approximation neglects completely the interference effects. Under this approximation the matrix elements in Table III can be transformed to intensities. These intensities are given in Table IV, where the intensities for the (close to) degenerate final states have been added. The overall intensities are given as

$$I(\Gamma,\Gamma') = |\langle 3s^1 3d^1[\Gamma']|r_q|2p^5 3d^1[\Gamma]\rangle|^2 \times |\langle 2p^5 3d^1[\Gamma]|r_q|3d^0\rangle|^2. \quad (2)$$

The 7×4 matrix of intensities is plotted in Fig. 1. The x axis gives the energies of the incoming x-ray energy and the y axis the energy difference of the incoming and outgoing energies. That is, on the x axis the $2p^5 3d^1$ states have constant energy and on the y axis the $3s^1 3d^1$ states have constant energies. The integral over the y axis gives the $2p$ x-ray absorption cross section. In Table IV also the ligand field nature and the spin nature of the seven $2p^5 3d^1$ states have been given. For example, the peak at the highest energy has 87% T_2 character and 13% E character;[19] it has 46% triplet character and 54% singlet character. All $3s^1 3d^5$ states are 100% pure in T_2 or E character and they are also very close to 100% pure in triplet or singlet character. This implies that the sum of the intensities of $2p^5 3d^1 \rightarrow 3s^1 3d^1[T_2]$ transitions is equal to the percentage of T_2 character of the intermediate states. This can be seen in Table IV and Fig. 1 where the T_2-like intermediate states decay essentially to T_2 final states.

TABLE III. All dipole transition matrix elements for the $3d^0 \rightarrow 2p^5 3d^1$ excitation and $2p^5 3d^1 \rightarrow 3s^1 3d^1$ decay. The signs are important for the interference effects.

Energy	$\langle 2p3d\rangle$	$^3E[T_1]$ 46.53	$^3E[T_2]$ 46.53	$^3T_2[T_1]$ 47.44	$^3T_2[E]$ 47.44	$^3T_2[T_2]$ 47.44	$^1E[E]$ 47.73	$^1T_2[T_2]$ 48.64
346.6	0.1059	−0.7413	−0.6344	−0.1061	0.1374	−0.0243	−0.1305	−0.0035
347.2	0.2598	0.4245	−0.3828	−0.1966	−0.2900	−0.1673	−0.6558	−0.3037
347.5	0.0597	0.1051	0.0891	−0.7226	0.4311	−0.4910	0.0985	0.1487
348.1	0.1632	0.1791	−0.0233	−0.1115	0.6378	0.6875	−0.2686	−0.0558
348.9	−0.8513	−0.2501	0.2623	−0.4959	−0.3068	0.2997	0.1870	−0.6353
350.9	0.3900	−0.3842	0.5894	0.1845	0.1726	−0.2548	−0.5994	−0.1294
353.3	1.0070	−0.1294	0.1616	−0.3678	−0.4247	0.3205	−0.2766	0.6797

TABLE IV. Intensities of excitation and decay obtained by squaring all matrix elements, multiplying excitation and decay and adding the degenerate final states.

Energy	Intensity	% E	Triplet	^3E 46.53	$^3T_2$ 47.44	^1E 47.73	$^1T_2$ 48.64
346.6	0.011	97%	98%	1068	34	19	.01
347.2	0.067	76%	48%	2205	1018	2903	622
347.5	0.003	3%	96%	6	339	3	7
348.1	0.026	10%	92%	87	2378	192	8
348.9	0.724	16%	56%	9524	31161	2536	29250
350.9	0.152	85%	62%	7532	1959	5467	254
352.3	1.014	13%	46%	4349	42439	7763	46865

The important consequence of this observation is that the final states map out the character E versus T_2 and singlet versus triplet of the intermediate states, thereby creating a direct experimental route to determine the character of the $2p$ x-ray absorption excitons. By setting the detector to a certain decay channel one can determine directly its spread over the x-ray absorption spectrum. This procedure has been used, for example, to separate spin-up and spin-down states in so-called ''local spin selective x-ray absorption.''[24] Similarly this can be used in the present case to obtain a T_2 symmetry projected x-ray absorption spectrum. There is one major problem in doing this, namely, that interference effects will tend to destroy this nice picture of a 100% pure decay channel. In fact it will be shown below that this destruction is very effective.

D. The importance of interference effects

Figure 2 gives the full result using the matrix elements of Table III and a Lorentzian broadening of 0.2 eV for the $2p$ holes and 0.4 eV for the $3s$ holes. A small Gaussian spread in the incoming x-ray energies of 0.25 eV has been used. Notice that as for Fig. 1 it has been chosen to plot $\omega-\omega'$ versus ω, instead of a ω' versus ω plot. The reason for this is that the constant final-state spectra are directly visible. At first sight Fig. 2 looks very much like a broadened version of Fig. 1, suggesting that interference effects are not dramatic for the actual IXS cross section (but see below).

In experimental studies it is customary to plot a spectral shape, that is a particular cross section of Fig. 2. Three often used spectral shapes are the following: (a) the resonant x-ray emission spectrum $I(\omega')|_\omega$, which is a cross section along the y axis. Experimentally this is the most common cross section because one only has to scan the detector with fixed incoming x-ray energy. The spectrum plotted as $I(\omega-\omega')|_\omega$ identifies with this cross section. The only difference is that the spectrum is shifted over ω, which is done in order to align identical final states if two excitation energies are compared. (b) The constant final-state spectrum $I(\omega)|_{\omega-\omega'}$ is a cross section along the x axis at a fixed point on the y axis in Fig. 2. With a constant final-state spectrum one can map out certain features of the intermediate states as indicated in the previous section. (c) The cross section $I(\omega)|_{\omega'}$, which is the detection of the excitation spectrum obtained at a fixed decay energy. This leads to a somewhat complex result. In Fig. 2 it identifies with a cross section taken at $-45°$, i.e., the same amount of change in $\omega-\omega'$ and ω.

In order to investigate more closely the importance of interference effects in Fig. 3 a series of spectra $I(\omega-\omega')|_\omega$ is plotted, where the excitation energy ω is chosen at the seven peaks of the absorption spectrum. The bottom spec-

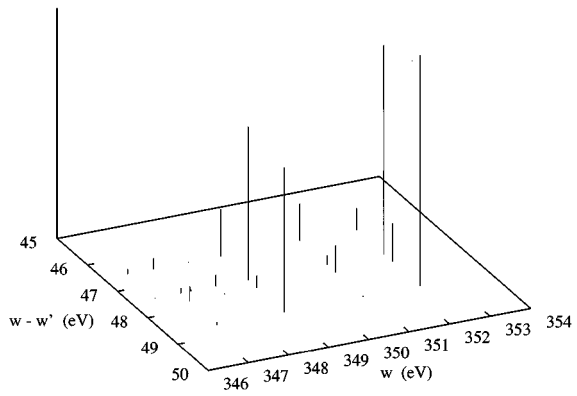

FIG. 1. Intensity line plot of the IXS cross sections, calculated as the x-ray absorption intensity times the x-ray emission intensity. Excitation energy (ω) on x axis; final-state energy ($\omega-\omega'$) on y axis. The seven $2p^5 3d^1$ intermediate states are visible along the x axis and the four $3s^1 3d^1$ final states are visible along the y axis.

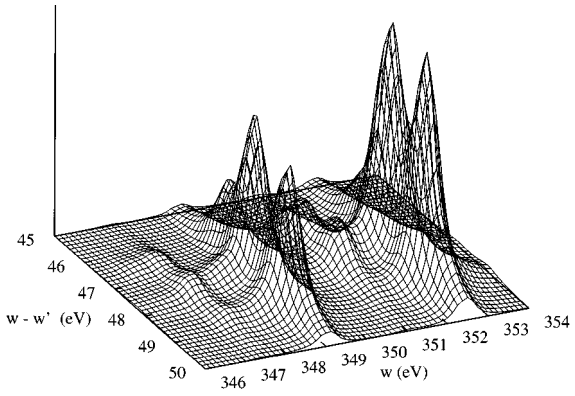

FIG. 2. Intensity plot of the IXS cross sections, calculated using Eq. (1), that is including interference effects. Excitation energy (ω) on x axis; final-state energy ($\omega-\omega'$) on y axis. A Gaussian broadening of 0.25 eV (HWHM) has been used, together with the lifetime broadenings $\Gamma_{2p}=0.2$ and $\Gamma_{3s}=0.4$ eV.

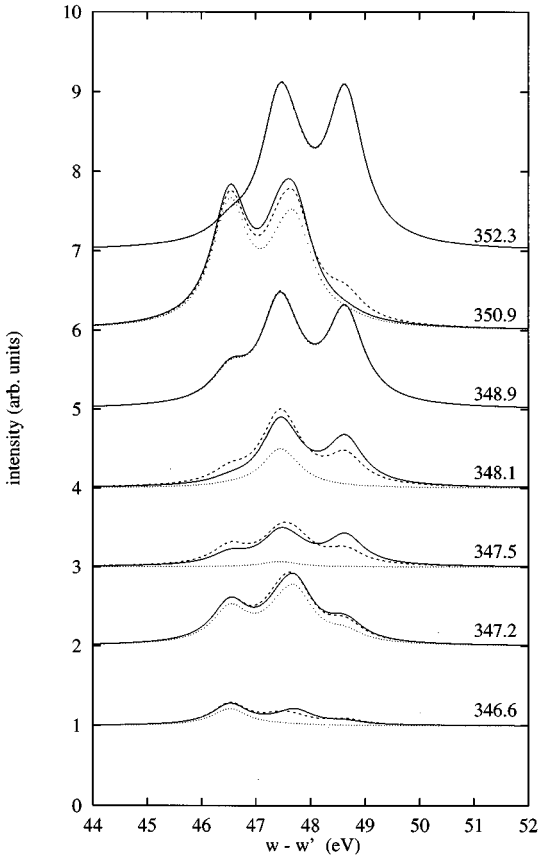

FIG. 3. Cross sections $I(\omega-\omega')|_{\omega}$ through Fig. 2 at the excitation energies indicated on the right. The dotted lines gives the decay of only the excited state at precisely the energy indicated. The dashed lines include the Lorentzian tails of the neighboring states and the solid lines include interference effects. The spectra with excitation energies at 348.9 and 352.3 have been divided by 5. Broadenings as in Fig. 2.

trum relates to the first small prepeak at 346.6 eV and the top spectrum relates to the highest peak at 352.3 eV. The spectra of the two large peaks at 348.9 and 352.3 eV have been reduced to 20% with respect to all other spectra. In Fig. 3 three sets of theoretical spectra are given. The spectrum indicated with dots is the decay spectrum of the particular intermediate state, which is excited. The dashed spectrum is the decay spectrum without interference but with the inclusion of the Lorentzian tails of the neighboring intermediate states at the energy of excitation. This spectrum will be indicated as the noninteracting superposition of Lorentzians. The solid spectrum is the spectrum for which interference effects have been included.

From Fig. 3 the following observations can be made: For the two main peaks in the excitation spectrum all three procedures to calculate the decay spectrum give identical results. This is easy to understand as there is one channel that completely dominates, hence the Lorentzian tails of the neighbors can be neglected. This implies that interference effects cannot be effective because then two channels are needed that have approximately the same size of effective matrix elements, that is a matrix element weighted by the lifetime broadening at a certain energy difference from the peak. There is a considerable interference for most small peaks, for example, the peak 350.9 eV (second from the top). This is the case because there is a considerable overlap of the Lorentzian tails of the two large peaks at both sides. Although the lifetime broadening is only 0.2 eV and the energy difference is 1.4 eV with the main peak at 352.3 eV, its intensity is a factor of 8 larger with the result that it still influences the excitation at 350.9 eV. The noninteracting superposition of the Lorentzian spectrum (dashed) clearly shows a shoulder at 48.6 eV, related to the influence of the tails of the main peak. However, this shoulder disappears again if interference is turned on (solid). The reason is that the interference for this 48.6-eV peak is destructive, as can be seen from Table III. Using the numbers in Eq. (1), one adds a negative number (0.39×-0.12) to a positive one (proportional to 1.0×0.67) and squares. Using Table III one deduces that the interference effects are constructive for the 47.7 state but destructive for all transitions to the 47.4 states. From Fig. 3 one can observe that the overall effect for the peak at 47.5 eV is constructive.

One can observe in Fig. 3 that in all comparisons of interference-on (solid) and interference-off (dashed) the integrated intensities of the solid and dashed line are equivalent, or in fact identical as the integrated intensity is conserved by a sum rule. Relatively large interference effects can be seen for the spectra excited at 347.5 and 348.1 eV. These two energies relate to weak excitations, hence the decay spectrum is dominated by the Lorentzian tails of the neighbours, which have 20 to 30 times more intensity at only 0.3 and 0.6 eV away. That is, interference effects are largest if two channels have a comparable effective strength at a certain energy.[31]

In conclusion, at all energies away from the main peaks the interference effects will be visible, especially at those energies with equivalent effective strengths. Interference effects can be destructive or constructive. This depends on the sign of the matrix elements for excitation and decay, as given in Table III.

E. The detection of specific decay channels

Above it has been argumented that it is possible to map out directly the amount of T_2 character, or triplet character, within the $2p$ x-ray absorption spectrum. Because the $3s^13d^1$ final states are (close to) 100% pure in ligand field and spin character, by putting the detector on such a final state one can map out its character. In this section it will be shown how this appealing picture is largely destroyed by interference effects.

A similar approach has been used for the $3p1s$ inelastic x-ray scattering cross sections of manganese compounds. The $3p^53d^5$ final states contain two energy regions almost pure in their spin character and separated by more than 10 eV.[24,32,33] This situation has been used to map out the spin-selective x-ray absorption states. In the present case of $3s2p$ inelastic x-ray scattering these T_2-selective or triplet-selective x-ray absorption spectra can be plotted directly by making a cross section through Fig. 2 along the x axis at a particular final state energy $\omega-\omega'$. These so-called constant-final-state spectra (cfs) are plotted in Fig. 4 for the energies related to the four $3s^13d^1$ final-state energies. For the curves in Fig. 4 both the overlap of the Lorentzians and

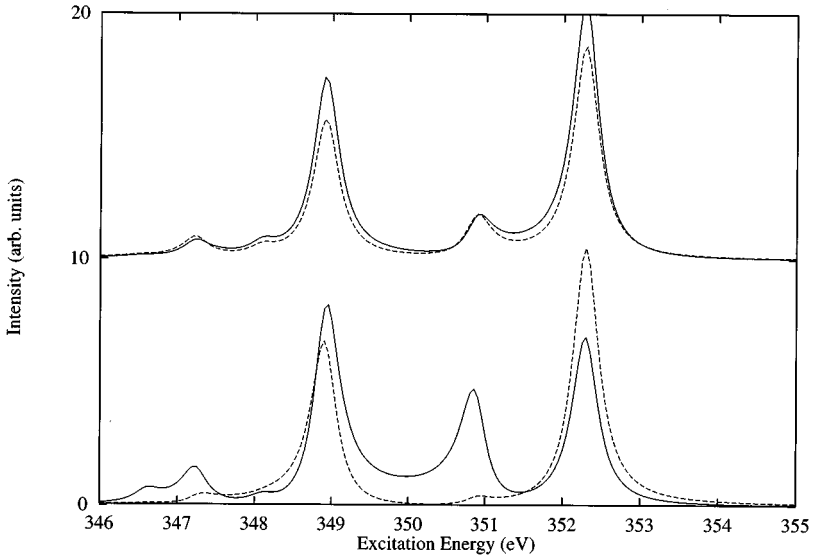

FIG. 4. Constant final-state spectra $I(\omega)|_{\omega-\omega'}$. Top: spectra for the ^1E state ($\omega-\omega'=47.73$ eV, dashed) and for the $^3T_2$ state ($\omega-\omega'=47.44$ eV, solid). Bottom: spectra for $^1T_2$ with $\omega-\omega'=48.64$ eV (dashed) and for ^3E with $\omega-\omega'=46.53$ eV (solid, multiplied by 2.5).

the interference effects have been included. These four curves should be compared with the numbers as given in Table IV. This comparison is correct for the $^1T_2$ peak detected at 48.64 eV. For the other decay channels it is wrong: The ^1E and $^3T_2$ channels at 47.73 and 47.44 eV are too close to each other to be separated, given the $3s$ lifetime broadening. It can be observed in Fig. 4 that both spectra are similar. In the case of the spectrum taken at $\omega-\omega'=46.53$ eV the Lorentzian tails of the neighboring peaks are too strong to relate the observed spectral shape quantitatively to the ^3E character. From these observations one can conclude that in the present the case only the $^1T_2$ peak at 48.64 eV can be used to map out the character of the intermediate states.

Concerning the broadening mechanism it is noted that in case of the $3p1s$ inelastic x-ray scattering cross sections the decay channel is also used to remove the lifetime broadening of the intermediate state,[23] or better, the $1s$ lifetime broadening of about 2.0 eV is replaced by the $3p$ lifetime broadening of about 0.4 eV. In the present case this implies that the $2p$ lifetime broadening of about 0.2 eV is replaced by the $3s$ lifetime broadening of 0.4 eV. In other words the spectrum becomes intrinsically broader instead of sharper. The actual situation is even worse due to the additional interference effects, which are not present for a $1s$ hole. From this analysis it is clear that the use of particular decay channels to map out a particular character should be used with great care. The final state used for the mapping must be separable from the other final states and the intermediate states at stake should also be in a situation insensitive to interference effects.

III. COMPARISON WITH EXPERIMENT

In this section the theoretical results will be compared to the experimental IXS spectra as measured by Rubensson *et al.* [21] They measured the $3s2p$ x-ray emission spectra at several positions within the $2p$ x-ray absorption edge. The experiments were done with a resolution of 0.6 eV [full width at half maximum (FWHM)] for the incoming x rays and 0.4 eV (FWHM) for the outgoing x rays. In Fig. 5(a) seven theoretical resonant $3s2p$ x-ray emission spectra are plotted. All spectra are given with their theoretical intensity including interference, that is by using Eq. (1). For convenience the seven spectra have been given an offset, chosen to be their excitation energy (minus 345 eV). Note that the photon energies are plotted and the energy axis runs in the opposite direction from Fig. 3.

In Fig. 5(b) the theoretical spectra are compared with the experimental spectra taken at the four main peaks at 347.4, 349.0, 350.9, and 352.3 eV in the experimental spectrum. The theoretical spectra are taken at the same energies, with the exception of the second peak, which is taken at 348.9 to be positioned exactly at the maximum of the peak. The theoretical spectra have been determined using Eq. (1), with lifetime broadenings $\Gamma_{2p}=0.2$ and $\Gamma_{3s}=0.45$ eV, convoluted with a Gaussian broadening of 0.27 eV (HWHM), chosen in order to mimic the experimental broadening. The experimental spectra are shown on the same scale. The theoretical spectra have been given a small flat background in order to reproduce the flat background of the experimental spectra. The highest peak is normalized to experiment and all other peaks are plotted with their theoretical intensity ratio. Also the energy position of the highest peak is aligned with experiment (because the multiplet calculations are always some eV wrong as far as absolute energies are concerned[2]).

Before discussing in detail the comparison between theory and experiment it is noted that in the theory all atomic parameters (Slater integrals) have been kept at their atomic values and the ligand field splitting has been kept at -0.91 eV as determined by x-ray absorption. No additional parameter enters the calculation, apart from the broadenings. Comparing theory and experiment, one notices the following things: (1) The spectral widths are equivalent, in particular there are in general two structures in each spectrum. (2) The relative shifts of the spectra are identical in theory and experiment. (3) The relative overall intensities are (with the exception of the 347.4-eV peak) similar. (4) There is an extra structure at a constant kinetic energy of 302.0 eV for the spectra excited at 350.9 eV and 352.3 eV. (5) The two main peaks have a double-peaked structure in the theory and only a shoulder in the experiment.

These five points will now be discussed in more detail. (1)

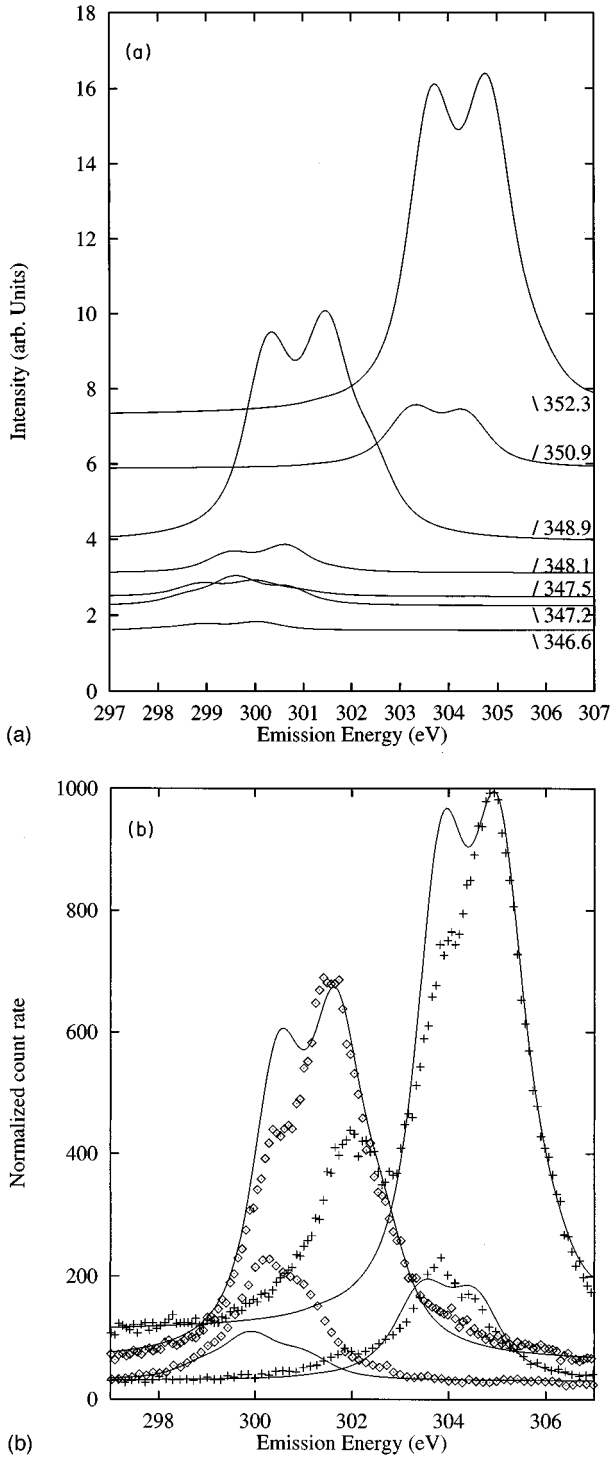

FIG. 5. (a) The resonant x-ray emission spectra $I(\omega')|_{\omega}$ at the excitation energies are given on the right. All intensities given on the same scale. (b) Comparison with experiment for the four main peaks in the absorption spectrum. The experimental spectra at 347.4 eV (small) and 349.0 eV (large) are given with diamonds. The spectra taken at 350.9 eV (small) and 352.3 eV (large) are given with crosses. The four theoretical spectra have an offset adapted to experiment. The series of four spectra are aligned and normalized at the peak-maximum of the 352.3 eV peak only.

That the overall widths agree is no surprise as the general model of the $3s^1 3d^1$ final states split by $3s3d$ exchange and ligand field is well known (and the theoretical spectra have been convoluted with a Gaussian to mimic the experiment). (2) The relative energy shifts are largely determined by the energy shifts between the excitation energies. The energy difference between the two largest spectra is exactly equal to this energy shift, because they reach the same two final states as discussed above. There is in theory and experiment exactly the same variation in the energy shifts as the E_g states reach different final states as the T_{2g} states. (3) That the relative intensities of all but the 347.4 spectrum are in close agreement between theory and experiment implies that the experiment detects a fluorescence yield that is proportional to the prediction with the model, in other words, it is proportional to the x-ray absorption intensity. Though this is no big surprise, it is noted that this is not always the case as has been shown for fluorescence yield detection using the $3d \rightarrow 2p$ emission.[34] Variations can in principle occur due to overall intensity fluctuations in some decay channels, which will to some extent influence all other channels. However, as noted above the $3s \rightarrow 2p$ is constant and the dominant Auger channels do show almost no variation (see Ref. 34 and references therein), thus the integrated intensity equals the x-ray absorption cross section. The fact that the intensity of the 347.4-eV peak is higher in experiment can be explained due to the relatively large contribution of surface-related states at this energy, as has been shown in Ref. 7. (4) As explained in Ref. 21 the extra peak at 302.0 eV is a consequence of the decay from the ionized state $2p^5\varepsilon$ reached directly or via Coster-Kronig decay. This will be discussed in the next section.

(5) Perhaps the most significant point is that the two largest spectra, related to the T_2 intermediate states at 348.9 and 352.3 eV, do show a clear double-peaked spectrum in theory, while in experiment they do show only a shoulder. The energy separation of the two peaks seems to be exactly correct but the intensity of the $^1T_2$ final state is too high as compared with the $^3T_2$ final state (plus the ^1E final state; cf. Table IV). There are several potential origins for this difference. (a) In the theoretical simulation a constant $2p$ lifetime broadening has been assumed that is known to be not exactly correct.[2] A different broadening will influence the degree of interference effects but as these effects are very small for the two main peaks (cf. Fig. 3) the estimated maximal effect is less than 1%. (b) Also the potential influence from surface-related states[7] can be expected to be very small, though they will have the correct tendency in lowering the $^1T_2$ states. (c) The model used in Ref. 21 assumes a variation in $3s3d$ exchange and also a variation in the ligand field splitting. For the peak ratio it is important to note that variations as large as 30% in the exchange interaction and ligand field interaction have an effect of only about 1% on the decay matrix elements. Thus even if these variations occur they will not affect significantly the intensities. (d) A large change in the relative intensity of the two peaks occurs when the excitation energy is shifted over the peak maximum. Shifts of only 0.1 eV can result in intensity variations of up to 10%. Knowing that the incoming x rays have a spread of 0.6 eV, this might cause some intensity variations, more if the intensity distribution of the incoming x rays does not follow a Gaussian. However, as the incoming x-ray energy is set exactly at the peak maximum this effect should be small. (e) Other possibilities include a difference in the effect of charge transfer

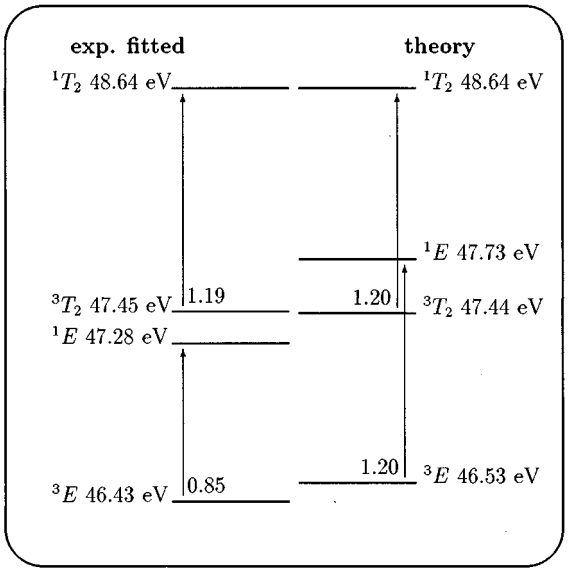

FIG. 6. $3s^13d^1$ final-state energy diagram, comparing the results fitted to experiment (left) and the ligand field multiplet (LFM) results (right). Experimental ligand field splittings are, respectively, 1.02 eV (triplet) and 1.36 eV (singlet), compared with the LFM value of -0.91 eV. The $3s3d$ exchange splittings are indicated with the arrows.

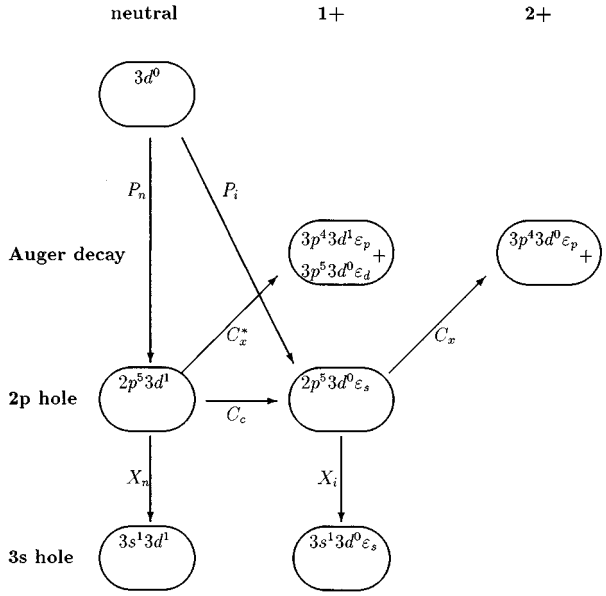

FIG. 7. Diagram indicating all relevant channels in which a $2p$ core hole is created and annihilated. Horizontally each column represents an ionization state as indicated at the top. Vertically each row represents a particular type of core hole as indicated on the left. The row indicated with Auger decay includes all possible configurations reachable by Auger decay from the $2p$ core hole. C indicates Auger decay, where C_c is a Coster-Kronig Auger transition. Both C_x and C_x^* indicate all Auger channels annihilating the $2p$ hole. P indicates x-ray absorption transitions and X x-ray emission decay, where the subscript n implies a neutral intermediate and final state and i an ionised $(1+)$ state. For example, a transition series can be $3d^0 \rightarrow 2p^53d^1 \rightarrow 2p^5\varepsilon_s \rightarrow 3s^1\varepsilon_s$.

(see Ref. 24). However, none of these effects seems to be large enough to explain this discrepancy by itself. Therefore no final conclusion can be reached to explain this difference between theory and experiment.

From the theoretical calculations a number of conclusions can be drawn that differ from the spectral analysis in Ref. 21. For example, a ligand field splitting of -0.91-eV is found in contrast to the fitted -1.02 eV (triplet) and -1.36 eV (singlet) values. The -0.91-eV value has been optimized to the $2p$ x-ray absorption spectrum, which was reproduced in great detail.[2] It is difficult to understand why the ligand field should be larger for a $3s^13d^1$ configuration than for the $2p^53d^1$ configuration. Also the large difference between singlet and triplet ligand field strengths is not supported by the $2p$ x-ray absorption spectrum, that is, both the $2p_{3/2}$ and $2p_{1/2}$ parts of the spectrum can be simulated accurately with exactly the same ligand field splitting. In the present multiplet model also a single exchange splitting of 1.2 eV states has been used (for both t_{2g} and e_g), while the experimentally fitted values are 0.85 (e_g) and 1.19 (t_{2g}) eV.

To show clearly the two different sets of $3s^13d^1$ peaks in Fig. 6 both the theoretical positions (right) and the experimentally optimized fits (left) are plotted. An important consequence from the theoretical numbers is that the ordering of states is different from the fitted one. The ^1E state is at lower binding energy than the $^3T_2$ state in the experimental fit. Because in the experimental fit there is no necessary condition on the symmetry of each peak it is possible to exchange the labels ^1E and $^3T_2$. Another possibility would be to refit experiment with the condition that the ligand field splitting be fixed to -0.91 eV for both triplet and singlet states. A consequence of the difference in assignment of the $3s^13d^1$ states is a large difference in the triplet to singlet intensity ratio of each of the $2p^53d^1$ intermediate states. The fitted results are that the T_2 states contain around 70% triplet character, whereas the result of the ligand field multiplet calculations are that both T_2 states have around 50% triplet character. Also the two largest E states have around 50% triplet character. The three low-intensity peaks are dominated by triplet character ($>92\%$). These theoretical percentages (cf. Table IV) have been determined without the inclusion of the Lorentzian tails and their interference effects.

The peak at 302.0 occurs at constant photon energy (ω') in contrast to all peaks discussed so far that occur at a constant binding energy ($\omega-\omega'$). As has been discussed in Ref. 21 the constant kinetic energy peak at 302.0 eV is related to radiative decay from an ionized $2p^5\varepsilon$ core hole, where ε denotes a free electron. The $2p^53d^1 \rightarrow 3s^13d^1$ decay intensity (I_n) is then compared with the decay from the ionized state $2p^5\varepsilon \rightarrow 3s^1\varepsilon$ (I_i). To make the analysis more transparant in Fig. 7 the situation of the creation and annihilation of a $2p$ core hole is sketched in as far as necessary for the analysis of the $3s2p$ IXS spectra. In this figure P_n is the $3d^0 \rightarrow 2p^53d^1$ dipole transition to a neutral final state and P_i relates to the ionizing $3d^0 \rightarrow 2p^5\varepsilon_s$ transition. This ionized final state, which also includes ε_d, is referred to as $1+$. Both states with the $2p$ core hole decay via $3s \rightarrow 2p$ matrix element. The overall intensity of X_n and X_i must be equal. The $2p^53d^1$ final state can decay via a Coster-Kronig Auger channel (C_c) to $2p^5\varepsilon_s$ if a $2p^5\varepsilon_s$ continuum state occurs at the same energy as a $2p^53d^1$ state. Apart from this channel

there are a series of other Auger decay channels, all annihilating the $2p$ core hole. They are, together with all other radiative decay channels, collected under the term C_x. The overall size of the Auger channels is larger for $2p^5 3d^1$ (C_x^*) compared to $2p^5\varepsilon_s$ (C_x) due to relatively strong decay channels involving the $3d$ electron.[34,35]

The complete flow diagram is sketched in Fig. 7. The neutral final state, or resonant, decay intensity (I_n) is given as $P_n X_n$. Taking account of other decay channels annihilating a $2p$ hole and the Coster-Kronig channel this number must be corrected with a factor $(1-C_c-C_x^*)$. The constant kinetic energy intensity (I_i) is given as $P_i X_i$. To this channel must be added the route via the Coster-Kronig decay. ($P_n C_c X_i$) and both channels must be corrected with $(1-C_x)$. From experiment it is known that for shallow core holes the Auger channels dominate over radiative channels. Neglecting the difference between C_x and C_x^* one obtains

$$\frac{I_i}{I_n} \sim \frac{[P_i + P_n C_{c,\,\mathrm{eff}}]}{[P_n](1-C_{c,\mathrm{eff}})}. \tag{3}$$

$C_{c,\mathrm{eff}}$ is an effective measure of the Coster-Kronig decay and its value is renormalized due to the removal of C_x. This equation has been used to analyze the intensity ratio of I_n and I_i.[21] A complication is that all channels involving $2p^5 3d^1$ intermediate states have a strong symmetry dependence in their decay channels. If one attempts to calculate all creation and annihilation processes theoretically, the Coster-Kronig decay poses a problem.

In case of CaF_2 it has been noticed[21,16,19] that Coster-Kronig transitions occur at energies lower than expected. One might expect the continuum states to start at an energy given by the energy difference of the $2p$ level and the bottom of the conduction band. From a combination of $2p$ photoemission (348.9 eV), valence-band photoemission (top at -8.0 eV) and optical spectroscopy (band gap is 12.1 eV) one deduces that the continuum states start at 348.9 + 12.1 − 8.0 = 353.0 eV.[21] However, there is clear evidence, both from $3s2p$ IXS and $2p3p3p$ resonant Auger, that at energies below 353.0 eV Coster-Kronig processes occur. In Ref. 19 the Coster-Kronig channels have been discussed in the framework of charge transfer. It has been shown that if the decay channel $2p^5 3d^1 \rightarrow 2p^5\varepsilon_s$ is forbidden because the energy difference (ΔE) is positive then in most cases the charge-transfer-induced channel $2p^5 3d^2\underline{L} \rightarrow 2p^5 3d^1\underline{L}\varepsilon_s$ is open because its energy difference is given as $\Delta E - U_{3d3d}$. The amount of charge transfer in CaF_2 is low because the $3d^1\underline{L}$ configuration is at an energy of the order of the band gap (12.0 eV) above $3d^0$. Thus this channel will have very low weight in the ground state and also in the $2p$ x-ray absorption final state.[19] It shows, however, that there are decay channels down to lower energies than expected from the single-particle picture. The detailed study of these decay channels needs further experiments such as the detection of a much finer grid of excitation energies measured with higher experimental resolution. Radiative decay channels such as $3s2p$-IXS and nonradiative channels such as $2p3p3p$ resonant Auger or $2p$ resonant photoemission will all show the evidence of these Coster-Kronig decay channels.

IV. CONCLUDING REMARKS

The calculation of the $3s2p$ inelastic x-ray scattering cross section has been given for CaF_2 by making use of a ligand field multiplet model. The different ingredients of the ligand field multiplet model such as symmetries, energies, and dipole matrix elements have been discussed in detail, including the different origins of the energy splittings such as the ligand field splitting, the $3s3d$ exchange splitting, and the $3d$ and $2p$ spin-orbit couplings. All necessary dipole matrix elements have been given and it has been shown that interference effects are not negligible.

The detection of specific decay channels to map out, for example, T_2 or triplet character of the $2p^5 3d^1$ intermediate states is explained. Theoretically this character can be determined precisely, but it is outlined that the experimental route, which exists in principle, is in practice largely troubled by overlap and interference effects.

The experimental results of Ref. 21 are reproduced with the ligand field multiplet model and the Kramers-Heisenberg equation of inelastic x-ray scattering. The theoretically determined values of the ligand field splitting (-0.91 eV) and the $3s3d$ exchange splitting (1.2 eV) differ from the results fitted to experiment. It is outlined that consistency of the model requires the ligand field strength to be -0.91 eV.

Coster-Kronig decay is observed, both in $3s2p$ IXS and $2p3p3p$ resonant Auger, at energies lower than expected from the accepted models. This remains a challenging problem, which needs to be resolved by a series of high-resolution $3s2p$ IXS and $2p3p3p$ resonant Auger experiments.

ACKNOWLEDGMENTS

This work was supported by the European Union program ''Human Capital and Mobility.'' I kindly thank Dr. J.E. Rubensson for making available in digital form his experimental data as published in Ref. 21. Also I would like to thank Professor G.A. Sawatzky, Dr. B.T. Thole, and Dr. J.E. Rubensson for discussions.

APPENDIX

The dipole selection rules, spin-orbit coupling, and crystal symmetry reduction all have consequences for the symmetries involved. Here some group theory results are reproduced from Sugano, Tanabe, and Kitamura.[28]

A. Multiplication table in atomic symmetry

A multiplication table is used to couple two electrons in different shells or to couple the L and S quantum numbers in spin-orbit coupling. In atomic symmetry it just states that if $L=1$ and $S=1$ then J can be 0,1 or 2; that $P \otimes D = P, D, F,$ etc.

The dipole selection rule states that the L-quantum number must be changed by one and that the spin is conserved ($\Delta S = 0$). Important is the selection rules for J, which state that $\Delta J = -1, 0, +1$, with the additional condition that J cannot be zero in both the initial and final state. From the sym-

metry point of view this implies that the dipole selection rule can be expressed exactly with $[P]$ symmetry.

B. Projection rules from atomic to cubic symmetry

The projection rules govern the splitting of atomic states under symmetry reduction to cubic symmetry. Both S and P states are not split, a d-electron is split into T_2 and E, etc. Note that the dipole selection rule can be represented in cubic symmetry with T_1 symmetry.

Atomic		Cubic	
Dimension	Name	Name	Dimension
1	S (0)	A_1	1
3	P (1)	T_1	3
5	D (2)	E, T_2	2+3
7	F (3)	A_2, T_1, T_2	1+3+3
9	G (4)	A_1, E, T_1, T_2	1+2+3+3

C. Multiplication table in cubic symmetry

The multiplication of irreducible representations in cubic symmetry: Consider for example a $^3T_2$ state. The spin-orbit coupling implies that first the triplet ($S=1$) state is projected to T_1, followed by a multiplication of T_1 with T_2 to give the four overall-symmetry states as quoted in the table below. The dipole operator has T_1 symmetry and the possible final states can be found by multiplying the initial-state symmetry with T_1.

	A_1	A_2	E	T_1	T_2
A_1	A_1	A_2	E	T_1	T_2
A_2	A_2	A_1	E	T_2	T_1
E	E	E	A_1A_2E	T_1T_2	T_1T_2
T_1	T_1	T_2	T_1T_2	$A_1ET_1T_2$	$A_2ET_1T_2$
T_2	T_2	T_1	T_1T_2	$A_2ET_1T_2$	$A_1ET_1T_2$

[1] C.T. Chen, Nucl. Instrum. Methods Phys. Res. Sect. A **256**, 595 (1987); Rev. Sci. Instrum. **63**, 1223 (1992).

[2] F.M.F. de Groot, J.C. Fuggle, B.T. Thole and G.A. Sawatzky, Phys. Rev. B **41**, 928 (1990).

[3] J.C. Fuggle and S.F. Alvarado, Phys. Rev. A **22**, 1615 (1980).

[4] D. Rieger, F.J. Himpsel, U.O. Karlsson, F.R. McFeely, J.F. Morar, and J.A. Yarmoff, Phys. Rev. B **34**, 7295 (1986); F.J. Himpsel, U.O. Karlsson, J.F. Morar, D. Rieger, and J.A. Yarmoff, Phys. Rev. Lett. **60**, 161 (1988).

[5] R.A. Heaton and C.C. Lin, Phys. Rev. B **22**, 3629 (1980).

[6] Y. Gao, T. Tiedje, P.C. Wong, and K.A.R. Mitchell, Phys. Rev. B **48**, 15 578 (1993).

[7] F.J. Himpsel, U.O. Karlsson, A.B. McLean, L.J. Terminello, F.M.F. de Groot, M. Abbate, J.C. Fuggle, J.A. Yarmoff, B.T. Thole, and G.A. Sawatzky, Phys. Rev. B **43**, 6899 (1991).

[8] F.M.F. de Groot, J. Electron. Spectrosc. **67**, 529 (1994).

[9] Two recent review papers are L.C. Davis, J. Appl. Phys. **59**, R25 (1986); J.W. Allen, in *Synchrotron Radiation Research*, edited by R.Z. Bachrach (Plenum, New York, 1992).

[10] L.H. Tjeng, C.T. Chen, J. Ghijsen, P. Rudolf, and F. Sette, Phys. Rev. Lett. **67**, 502 (1991).

[11] G. van der Laan, M. Surman, M.A. Hoyland, C.F.J. Flipse, B.T. Thole, Y. Seino, H. Ogasawara, and A. Kotani, Phys. Rev. B **46**, 9336 (1992); G. van der Laan, B.T. Thole, H. Ogasawara, Y. Seino, and A. Kotani, *ibid.* **46**, 7221 (1992).

[12] M.F. López, A. Höhr, C. Laubschat, M. Domke, and G. Kaindl, Europhys. Lett. **20**, 357 (1992); L.H. Tjeng, *ibid.* **23**, 535 (1993); M.F. López, C. Laubschat, and G. Kaindl, *ibid.* **23**, 538 (1993).

[13] L.H. Tjeng, C.T. Chen, P. Rudolf, G. Meigs, G. van der Laan, and B.T. Thole, Phys. Rev. B **48**, 13 378 (1993).

[14] J.H. Park, L.H. Tjeng, R. Claessen, J.W. Allen, and C.T. Chen (unpublished); J.H. Park *et al.* (unpublished).

[15] T. Tiedje, K.M. Colbow, D. Rogers, and W. Eberhardt, Phys. Rev. Lett. **65**, 1243 (1990); Phys. Scr. **41**, 621 (1990).

[16] M. Elango, A. Ausmees, A. Kikas, E. Nommiste, R. Ruus, A. Saar, J.F. van Acker, J.N. Andersen, R. Nyholm, and I. Martinson, Phys. Rev. B **47**, 11 736 (1993).

[17] A. Kikas, A. Ausmees, M. Elango, E. Nommiste, R. Ruus, and A. Saar, J. Electron. Spectrosc. **68**, 287 (1994).

[18] M.F. López, C. Laubschat, A. Guttiérrez, A. Höhr, M. Domke, G. Kaindl, and M. Abbate, Z. Phys. B **95**, 9 (1994).

[19] F.M.F. de Groot, M. Elango, and R. Ruus, Phys. Rev. B **51**, 14 062 (1995); F.M.F. de Groot, Solid State Commun. **96**, 881 (1995).

[20] A. Mori, Y. Kayanuma, M. Nakazawa, and A. Kotani, J. Phys. Soc. Jpn. **63**, 306 (1994); A. Mori, Y. Kayanuma, and A. Kotani, Prog. Theor. Phys. **106**, 75 (1991).

[21] J.E. Rubensson, S. Eisebitt, M. Nicodemus, T. Böske, and W. Eberhardt, Phys. Rev. B **49**, 1507 (1994); J.E. Rubensson, S. Eisebitt, M. Nicodemus, T. Böske, and W. Eberhardt, *ibid.* **50**, 9035 (1994).

[22] K. Hämäläinen, C.C. Kao, J.B. Hastings, D.P. Siddons, L.E. Berman, V. Stojanoff, and S.P. Cramer, Phys. Rev. B **46**, 14 274 (1992).

[23] K. Hämäläinen, D.P. Siddons, J.B. Hastings, and L.E. Berman, Phys. Rev. Lett. **67**, 2850 (1991).

[24] F.M.F. de Groot, S. Pizzini, A. Fontaine, K. Hämäläinen, C.C. Kao, and J. Hastings, Phys. Rev. B **51**, 1045 (1995).

[25] P. Carra, M. Fabrizio, and B.T. Thole, Phys. Rev. Lett. **74**, 3700 (1995).

[26] J. Tulkki and T. Aberg, J. Phys. B **13**, 3341 (1980); **15**, L435 (1982).

[27] T. Aberg and B. Crasemann, in *X-Ray Anomalous (Resonance) Scattering: Theory and Experiment*, edited by K. Fisher, G. Materlik, and C. Sparks (Elsevier, Amsterdam, 1994).

[28] For an introduction to the group theory necessary for transition metal systems see S. Sugano, Y. Tanabe, and H. Kitamura, *Multiplets of Transition Metal Ions* (Academic, New York, 1970).

[29] R.D. Cowan, *The Theory of Atomic Structure and Spectra* (University of California Press, Berkeley, 1981).

[30] P.H. Butler, *Point Group Symmetry Applications: Methods and Tables* (Plenum, New York, 1981).

[31] If two channels have equal strength the interference effects can be $\pm$ 100% ($1^2 + 1^2$ vs 2^2 or 0^2). If one channel is only 10% of the other the maximum interference effect is only 20% ($10^2 + 1^2$ vs 11^2 or 9^2).

[32] P.S. Bagus, A.J. Freeman, and F. Sasaki, Phys. Rev. Lett. **30**, 851 (1973).
[33] G. Peng, F.M.F. de Groot, K. Hämäläinen, J.A. Moore, X. Wang, M.M. Grush, J.B. Hastings, D.P. Siddons, W.H. Armstrong, O.C. Mullins, and S.P. Cramer, J. Am. Chem. Soc., **116**, 2914 (1994).
[34] F.M.F. de Groot, M.A. Arrio, Ph. Sainctavit, Ch. Cartier, and C.T. Chen, Solid State Commun. **92**, 991 (1994).
[35] A. Tanaka and T. Jo, J. Phys. Soc. Jpn. **63**, 2788 (1992).